Deep-marine brine seeps stimulate microbial nitrogen cycling: implications for the formation of sediment-hosted ore deposits

Eva E. Stüeken[1,*], Annabel Long[1], Nathan Rochelle-Bates[1], Andreas Teske[2]

1. University of St Andrews, School of Earth & Environmental Sciences, Bute Building, Quen's Terrace, St Andrews, Fife, KY16 9TS, United Kingdom
2. University of North Carolina at Chapel Hill, Department of Marine Sciences, Chapel Hill, NC 27599-3300, United States of America
* corresponding author (ees4@st-andrews.ac.uk)

Key Points

- Brine seeps in the Gulf of Mexico recycle bioavailable nitrogen from sediments back into the water column.
- Nitrogen isotopes suggest that brine seepage stimulates biological activity, including dissimilatory nitrate reduction to ammonium.
- Biological productivity stimulated by brine seeps may have contributed to the formation of sedimentary ore deposits.

Abstract

Deep-marine brine seeps in the modern ocean are considered analogues for settings that favoured the formation of sedimentary-exhalative zinc and lead deposits in deep time. Microbial activity plays an important role in the accumulation of ore minerals, meaning that the extent of mineralization is at least indirectly dependent on nutrient fluxes. Here, we investigated the biogeochemical nitrogen cycle in shallow (15-50 cm) sediment cores from the Orca Basin brine pool and surrounding sites, as well as from an active brine seep area near Dead Crab Lake in the Gulf of Mexico, with the aim of constraining the effect of brine seepage on this bio-essential element. We find high porewater ammonium concentrations in the millimolar range, paired with elevated ratios of organic carbon to nitrogen in sediments, which confirm previous hypotheses that the brine recycles ammonium from sedimentary strata back into the water column. Within Orca Basin, we note tentative evidence of microbial ammonium utilization. At the active seep, ammonium is mixed into the overlying water column and likely undergoes oxidation. Isotopic data from sediments and dissolved ammonium, paired with previously published genomic data, suggest the presence of dissimilatory nitrate reduction to ammonium (DNRA) at the brine-seawater interface. We conclude that brine seeps can stimulate biological nitrogen metabolisms in multiple ways.

Our results may help calibrate studies of biogeochemical cycles around brine seeps that are archived in the rock record.

Plain Language Summary

Brine seeps in the deep ocean are sites where fluids with exceptionally high salinity, up to ten times that of seawater, seep up through marine sediments and are dispersed into the water column. Such saline fluids can carry high concentrations of metals such as iron, zinc, lead and copper, and therefore brine seeps have been proposed as mechanisms for the formation of ore deposits in the past. An important aspect in this theory is that high microbial activity near the brine seeps creates locally anoxic conditions under which metals are trapped in sulfide minerals. Such biological activity would require input of nutrients, including nitrogen. To shed more light on the biogeochemical nitrogen cycle in brine seeps, we investigated nitrogen isotopes and abundances in samples from the Gulf of Mexico. Here, ammonium concentrations in the millimolar range have previously been documented. Our results support the idea that nitrogen is leached by the brines from deeper sediments and released into the overlying water column. Furthermore, we find evidence for specific microbial metabolisms that are stimulated by mixing between anoxic brine fluids and oxygenated seawater, which may also have occurred in past ore-forming environments.

1. Introduction

Anoxic brine pools and saline seeps at the bottom of the ocean with salinities nearly ten times that of seawater are some of the most extreme environments on the modern Earth (Mapelli et al., 2017; Merlino et al., 2018). They are inhabited by a plethora of microorganisms that capitalize on strong gradients in redox conditions and metabolic substrates. High sulfide concentrations within the brine attest to extensive microbial sulfate reduction, coupled to the oxidation of methane or larger hydrocarbons (Boetius et al., 2005; Lloyd et al., 2010), while sulfide-oxidizing bacteria thrive at the seawater-brine interface on sediment surfaces (Sassen et al., 1993; Teske and Carvalho, 2020). The well-documented, active sulfur cycle makes these environments potential analogues for the formation of sedimentary exhalative (SEDEX) ore deposits in the rock record, where genetic models postulate injection of metal-rich brines into seawater, followed by the generation of anoxic brine pools and trapping of base metals in sulfide minerals (Emsbo, 2009; Sangster, 2018). A famous example is the world-class Pb-Zn

SEDEX deposit in the late Paleoproterozoic McArthur Basin (1.6 Ga), where saline brines enriched in metals are thought to have originated from older evaporites deeper within the basin (Large et al., 1998). In this case, a steep geothermal gradient likely facilitated fluid convection and seepage of metal-rich brine into overlying anoxic strata and/or into the water column where sulfide minerals were deposited (Ireland et al., 2004; Williams, 1978).

It has been proposed that the hydrothermal saline seeps of the McArthur Basin also carried with them re-mobilized hydrocarbons (Williford et al., 2011) and ammonium (Stüeken et al., 2021). The latter in particular could have constituted an important source of bioavailable nitrogen to the biosphere, to alleviate N-limitation during the mid-Proterozoic (Anbar and Knoll, 2002). Stimulation of microbial activity by ammonium may have further enhanced anoxia, sulfate reduction and metal accumulation. Indeed, modern saline seeps and brine pools are highly enriched in ammonium with concentrations up to 11 mM (Joye et al., 2005; Joye et al., 2010), supporting the idea that such seeps may act as important nutrient point sources. However, our ability to draw comparisons to ancient settings is limited by the lack of detailed investigations of microbial nitrogen cycling in modern environments, in particular with regards to isotopic signatures that can be preserved in the sedimentary record.

To fill this knowledge gap, we measured nitrogen isotopes, along with organic carbon isotopes and ratios of organic carbon to nitrogen in sediment samples from modern saline seeps environments in the Gulf of Mexico. Electrical conductivity, as well as pore fluid concentrations and the isotopic composition of ammonium, were measured to be able to link sedimentary signatures to fluid properties. Our results support the notion that saline seeps act as a recycling mechanism that remobilizes ammonium from sediments (Joye et al., 2005; Joye et al., 2010) and stimulates microbial activity at the brine-seawater interface and possibly at regional scale.

2. Study Site

The Gulf of Mexico is partially underlain by salt deposits of Jurassic age that have been deformed into diapirs over nearly 200 million years by tectonism, geothermal heating, and differential loading as the sedimentary overburden has accumulated (Joye et al., 2005; Peel et al., 1995; Pindell and Kennan, 2009). Faults act as fluid conduits along which seawater

penetrates into the subsurface and partially dissolves the salt bodies, forming highly saline brines. Geothermal heating creates buoyancy, causing the brines to rise and seep into the basin along faults with temperatures ca. 10-15°C above ambient background (Joye et al., 2005; Roberts and Carney, 1997). Such saline seeps occur in multiple localities around the northwestern Gulf Basin. The most famous locality is the Orca Basin, which is the world's largest submarine brine pool with a maximum depth of 600 m below the surrounding seafloor and a surface area of ca. 400 km^2 (Pilcher and Blumstein, 2007; Shokes et al., 1977).

Samples for this study came from three distinct sites (Fig. 1, see supplementary tables for site coordinates in lat/long). The first set of samples (5 cores), collected by HOV Alvin during dive 4650 represents an active brine seep near Dead Crab Lake, a small brine pool (ca. 10 m across) in the Green Canyon area in the Gulf of Mexico (Teske and Joye, 2020). At the time of sample collection in 2010, the surficial sediments at this location harbored sulfur-oxidizing microbial mats (Stevens et al., 2015; Teske and Carvalho, 2020). Also one brine sample from Dead Crab Lake was collected. The second sample set (3 cores, hereafter referred to as slope setting) was collected by HOV Alvin (Dive 4650) at the slope of Orca Basin, rising from sediments near the oxycline and halocline that do not contain visible benthos ("Pink Jello" core 4560-5, 2198 m and "red core" 4560-24, 2186 m) towards oxic conditions above the halocline and oxycline, evidenced by benthic macrofauna in the form of sponges ("Sponge Garden", core 4650-3, 2167 m). These characteristics attest to gradually increasing oxic conditions in the water column within this sample set (Nigro et al., 2020). Our third sample set was obtained by multicorer sampling from the consistently hypersaline and anoxic bottom sediments of Orca Basin (Nigro et al., 2020). One core is from the south sub-basin (MUC-6), and one additional sediment sample comes from the north sub-basin (MUC-7). In addition, we obtained five samples of the brine lake (CTD cast 0502 and Alvin dive 4647). The sediment cores from the three samplings sites were ca. 15-50 cm in length and subdivided into 2-5 cm sections, which were analysed separately as individual samples. Whenever feasible, sampling sites were recorded with *Alvin's* external camera and automated screen grab system (4dgeo.whoi.edu, Fig. 1).

3. Analytical Methods

After collection (Nigro et al., 2020; Teske and Joye, 2020), the samples were stored in the freezer at the University of North Carolina at -80°C. For this project, the frozen samples were

shipped to St Andrews in the UK on ice packs. Immediately after arrival, they were fully thawed and then centrifuged at 3000 rpm for 10 minutes. The pore waters were passed through 0.2 µm PTFE syringe filters (which were washed three times with DI-water), acidified with 100 µl of 1M HCl to limit ammonia (NH_3) gas loss, stored in separate Falcon tubes and subsequently kept frozen. The solid sediment residues were placed into a freeze drier for 2-4 days. Once dried, the sediments were pulverized to a fine powder with pestle and mortar and stored in Falcon tubes.

3.1. Sediment decarbonation

Ca. 0.5 g of powdered sediment sample were weighed out into pre-combusted (500 ℃) glass tubes, mixed with 1 M HCl (10-15 ml) and left overnight at room temperature, with loose caps to allow CO_2 degassing. The samples were then centrifuged at 700 rpm for 15 minutes and the acid was decanted. To ensure complete decarbonation, 1 M HCl was added again for 30 minutes. If effervescence was observed the samples were left in acid again overnight. After decanting the acid, the samples were washed three times in DI-H_2O (18.2 MΩ·cm) and then left to dry at 70 ℃ for three days before transfer into pre-combusted scintillation vials.

3.2. Organic carbon and nitrogen analyses of sediments

For analyses of total organic carbon and nitrogen content as well as isotopic ratios, ca. 10-15 mg of decarbonated sediment powder were weighed into tin capsules (8 mm height, 5 mm diameter; Elemental Microanalysis) and analysed by flash-combustion with an elemental analyser (EA Isolink; Thermo Fisher) coupled via a Conflo IV to a MAT253 isotope ratio mass spectrometer (Thermo Fisher). The EA was equipped with a combustion column packed with Cr_2O_3 and silvered cobaltous cobaltic oxide (held at 1020 °C), followed by a reduction column packed with Cu (held at 650 °C) and a water trap packed with magnesium perchlorate (held at room temperature). The GC column of the EA was ramped from 40 °C to 240 °C during each analysis to accelerate elution of CO_2. The data were calibrated for carbon and nitrogen abundances using a series of USGS-41a standards. Isotopic ratios were calibrated with USGS-41a and USGS-40. The results are expressed in delta notation relative to VPDB for carbon ($\delta^{13}C = [(^{13}C/^{12}C)_{sample}/(^{13}C/^{12}C)_{standard} - 1]\times1000$) and relative to air for nitrogen ($\delta^{15}N = [(^{15}N/^{14}N)_{sample}/(^{15}N/^{14}N)_{standard} - 1]\times1000$). USGS-62 and SDo-1 were analysed for

quality control, and the measured results (USGS-62: $\delta^{13}C$ = -14.79 ± 0.07 ‰ (1SD), $\delta^{15}N$ = 20.38 ± 0.17 ‰ (1SD), n = 30; SDo-1: $\delta^{13}C$ = -30.25 ± 0.04 ‰ (1SD), $\delta^{15}N$ = -0.53 ± 0.27 ‰ (1SD), n = 15) are in good agreement with expected values (USGS-62: $\delta^{13}C$ = -14.79 ± 0.04 ‰, $\delta^{15}N$ = 20.17 ± 0.06 ‰; SDo-1: $\delta^{13}C$ = -30.0 ± 0.1 ‰, $\delta^{15}N$ = -0.8 ± 0.3 ‰) (Dennen et al., 2006; Schimmelmann et al., 2016).

3.3. Ammonium quantification in pore waters

A colorimetric method based upon Cleaves *et al.* (2008) was used to determine the concentration of dissolved ammonium (NH_4^+) in pore waters. Analysis of the samples were carried out using the Thermo Fisher Scientific Evolution Series 200 UV-Visible Spectrophotometer at a wavelength of 640 nm. All reagents were prepared using pre-combusted glassware (500 °C) and DI-H_2O (18.2 MΩ·cm), including the sodium citrate buffer (7.6 g of trisodium citrate and 0.4 g of sodium hydroxide in 500 ml of DI-water), phenol alcohol (1 ml liquified phenol with 90 ml of 100% ethanol, brought up to 100 ml using DI-water) and aqueous sodium nitroprusside (0.15 g of sodium nitroprusside dissolved in 200 ml of DI-water). These were stored in the fridge for several weeks. Further, an oxidising solution was prepared daily from 10 ml of the sodium citrate buffer and 0.1 ml of aqueous sodium hypochlorite (10-15% available chlorine). A series of standards ranging from 0.5 µM to 100 µM was prepared to calibrate the method, using a stock solution of 1 mM NH_4Cl. Samples were diluted with DI-H_2O to fall within this range. To each 1 ml of standard or sample, 0.5 ml of phenol alcohol, 0.5 ml of aqueous sodium nitroprusside and 1 ml of oxidising solution were added within 15 ml Falcon tubes. The mixture was left to sit at room temperature for 60-80 minutes and then transferred to cuvettes for analysis. Average reproducibility was 1.6 % with a maximum of 8 %.

3.4. Ammonium microdiffusion method for dissolved NH_4^+ isotopic analysis

In a subset of samples from the active seep near Dead Crab Lake and from the Orca Basin brine pool, we analysed the isotopic composition of the dissolved ammonium using a microdiffusion method. Here, dissolved NH_4^+ of a sample is converted to NH_3 gas by addition of MgO and then trapped as NH_4^+ on an acidified glass fibre filter, which is subsequently analysed for isotopic composition. We adopted the protocol of Zhang *et al.* (2016). First, glass fibre filter disks with a diameter of 5 mm were cut from a 10 mm diameter Whatman

GF/D filter using a hole punch (cleaned with methanol). The disks were then placed on a 5×1 cm^2 strip of Teflon tape, and 10 µl of 2.5 M H_2SO_4 were pipetted onto the disk. Using tweezers, the Teflon tape was folded and sealed around the disk with the odd end of a pipette tip. Excess Teflon tape around the edges was cut off with scissors.

Solutions containing dissolved ammonium were diluted with DI-water to ammonium concentrations of 100 µM in a 10 ml volume. The dilutions were done in 20 ml glass vials. To maintain a balanced osmotic gradient across the Teflon tape and prevent rupture of the acid traps, 0.7455g of KCl (Sigma-Aldrich, Cat No. 7447-40-7) were added to each vial to achieve a 1 M concentration. Then one acid trap was added to each vial along with a magnetic stir bar (approximately 5 mm in length). Ca. 100 mg MgO (ThermoScientific, Cat No. 205155000) were added, and the vials were capped immediately with a septum and crimp cap. The mixture was then shaken to help homogenise the MgO in the solution. The vials were placed on magnetic stir plates in sand baths at 70 °C for four days. After incubation, the acid traps were removed from the vials, dipped in 1 M HCl, and briefly rinsed with DI-H_2O. The Teflon tape was pulled open, and the filters were placed into a freeze-drier for two days. Blanks with no ammonium addition were prepared in the same way. Further, a 'freeze-drier blank' acid trap was placed into the freeze drier to ensure that no absorption of ammonia gas occurred during the drying process. Three international ammonium sulphate standards were used for calibrating this method (IAEA-N-1, IAEA-N-2, and USGS-25). For each one, we prepared a 15 ml stock solution of 1 mM ammonium and doped it with 10 µl of 1 M HCl to prevent loss of ammonia gas during storage. For all samples and standards, the dried filters were transferred into tin capsules and analysed by the same EA-IRMS setup as the sediment samples. IAEA-N2 and USGS-25 were used to calibrate the isotopic ratios and IAEA-N1 was used for quality control. The measured results ($\delta^{15}N = 0.22 \pm 0.34$ ‰, n = 8) are in good agreement with the expected value ($\delta^{15}N = 0.43 \pm 0.14$ ‰) (Gonzalez and Choquette, 2023).

3.5. Electrical conductivity

For each sample site, one core was selected to measure the electrical conductivity (EC) of the pore fluids. These measurements were done with a Hanna EC probe, connected to a Hanna benchtop multi-meter. Prior to analyses, the probe was calibrated with a series of conductivity standards from Hanna, ranging from 84 µS/cm to 80'000 µS/cm. A 30 ml volume of each sample was prepared with a 100-times dilution in plastic 50 ml centrifuge tubes. The conductivity reading was taken once the reading had stabilized.

4. Results

The electrical conductivity profiles from representative sediment cores at the three sampling sites (Table 1, Fig. 2) show consistently high values (524-550 mS/cm, Fig. 2c) within the Orca Basin brine pool sediments and consistently low values in the slope sediments from and above the oxycline (79-83 mS/cm, Fig. 2b). The active seep near Dead Crab Lake shows a gradient from 182 mS/cm at the top to 419 mS/cm at the bottom of the core (Fig. 2a). These are consistent with visual observations of dense, reducing brine filling the coring holes during sampling and confirm the distinct characters of the three sampling sites.

The $\delta^{15}N$ values of the sediment samples (Table 2) from the Orca Basin slope (mean = 3.0 ± 0.7 ‰, 1SD) as well as from the Orca Basin bottom sediment (2.7 ± 0.2 ‰) (Fig. 3) are similar to the composition of dissolved nitrate in seawater in the Gulf of Mexico (2.5 ‰,Meckler et al., 2011). Only slope core 4650-3 above the oxycline ("Sponge Garden") is overall slightly enriched in ^{15}N to ca. 3.5 ‰ (removing this core from the mean reduces the average composition of the slope sediments to 2.7 ± 0.5 ‰). Organic carbon isotopes ($\delta^{13}C$) are similarly stable and show only a subtle difference between the Orca Basin slope (-22.7 ± 0.7 ‰) and the brine pool sediment (-21.8 ± 0.1 ‰). Molar ratios of organic carbon to total nitrogen (hereafter C/N) for the two sites are all between 10 and 13 (brine pool: 10.2 ± 0.1; slope site: 11.0 ± 0.7).

At the active seep near Dead Crab Lake, the sediments display $\delta^{15}N$ values only slightly above seawater nitrate in the bottom of all cores (Fig. 4), but in the top 5-10 cm, all cores show a shift towards lighter values where the minimum value always occurs in the top-most sample and ranges from -1.5 ‰ to +0.3 ‰ across the five cores. Organic $\delta^{13}C$ decreases in parallel with $\delta^{15}N$. At the bottom, all cores show $\delta^{13}C$ values around -26 ‰ to -27 ‰, while the core tops decrease to values around -30 ‰ or less. The lowest value of -41.4 ‰ is found 2-3 cm below the surface in core 4652-5. Molar C/N ratios are mostly above 10 at depth in all cores, but the core tops show a consistent decrease in C/N with a minimum of 7 found at the top of core 4652-5. As a consequence, $\delta^{15}N$ and C/N are strongly correlated across the active seep site ($R^2 = 0.65$, $p < 10^{-12}$).

When the total N (TN) content of the decarbonated residues is plotted versus total organic carbon (TOC) (Fig. 5), we find that the samples from the Orca Basin brine pool and the slope site fall along a continuum, attributable to their consistent C/N ratios. TN and TOC across all samples from both sites are strongly correlated ($R^2 = 1.0$, $p < 10^{-50}$) with a TN intercept of -0.01 wt. % (Fig. 5). In the sediments from the active seep near Dead Crab Lake, we find that the core tops with C/N < 10 fall along a steeper slope compared to the core bottoms with C/N > 10. In both cases, the two parameters are strongly correlated (R^2 = 0.99 and 0.83, respectively, $p < 10^{-6}$). The TN intercept is +0.02 wt. % in the subsurface and -0.09 wt. % in the core tops.

Dissolved ammonium in pore waters (Table 2) is mostly below 0.3 mM in the sediments from the Orca Basin slope; only few outliers exceed this threshold (Fig. 3). The mean is 0.16 + 0.28/-0.16 mM (median 0.09 mM). Brine samples from within 100 m of the surface of the Orca Basin Brine pool are slightly enriched in ammonium to up to 0.5 mM in the northern sub-basin (Table 3). Within the Orca Basin brine pool sediments, dissolved ammonium concentrations display a mean of 1.38 ± 0.14 mM. For the Orca Basin brine pool and porewater samples, we were able to obtain $\delta^{15}N$ isotopic measurements of the dissolved ammonium and found most of the sedimentary samples to cluster around a mean of 4.5 ± 0.3 ‰, systematically offset from the solid sedimentary values by 1.8 ± 0.3 ‰ on average. The top-most pore water sample is an outlier with a $\delta^{15}N$ value of 8.6 ± 0.5 ‰ for dissolved ammonium, confirmed with a replicate measurement (Fig. 6). This value is offset from the corresponding sediment by 5.7 ± 0.5 ‰. The brine from the overlying basin (5.2 ± 0.1 ‰ and 4.5 ± 0.2 ‰ at the two sites) is only slightly enriched in composition to the lower sedimentary pore waters.

In the sediments from the active seep area near Dead Crab Lake, dissolved ammonium concentrations broadly decrease up-section in all cores (Fig. 4). The gradient, defined here as the ratio of the maximum ammonium concentration at the base of each core to the minimum concentration at the top, ranges from 2.1 to 4.6. The highest concentrations with up to 8.5 mM were measured in core 4652-5 with a gradient of 3.3. For comparison, the gradient in electrical conductivity in the same pore fluids is 2.3 (Fig. 2). From this core, we also obtained isotopic data for the dissolved ammonium (Fig. 4). In the lower part of the core, the dissolved ammonium is offset in $\delta^{15}N$ from the sediments by 0.9 ± 0.2 ‰ on average, but the offset increases to up to 4.6 ± 0.6 ‰ at the top. In other words, the dissolved ammonium shows a more subtle decrease in $\delta^{15}N$ at the top of the core by only about 1 ‰ compared to a decrease

by ca. 4.5 ‰ seen in the sediment samples over the same interval. The brine sample from Dead Crab Lake is similar to the upper pore waters, showing a value of 3.3 ± 0.1 ‰.

5. Discussion

5.1. Sedimentary archive of marine nitrate in Orca Basin

The Gulf of Mexico is generally described as oligotrophic with high rates of biological N_2 fixation occurring in surface waters, making it a net source of fixed nitrogen to the global ocean (Gruber and Sarmiento, 1997). Biological N_2 fixation generates biomass with an isotopic composition around -1 ‰ (Carpenter et al., 1997; Minagawa and Wada, 1986). As this biomass is remineralized during sinking through the oxic water column, it is rapidly oxidized to nitrate, which adopts the same isotopic composition (Marconi et al., 2019). Globally, the marine nitrate pool is slightly enriched in ^{15}N due to partial nitrate reduction (denitrification) to N_2 in oxygen-minimum zones, giving it an average $\delta^{15}N$ value of ca. 5 ‰ (Brandes and Devol, 2002; Sigman et al., 2000). Mixing between nitrate from the open Atlantic and nitrate regenerated from biomass locally thus explain the $\delta^{15}N$ value of ca. 2.5 ‰ for nitrate dissolved in water column in the Gulf of Mexico (Knapp et al., 2005; Meckler et al., 2011).

This value of 2.5 ‰ closely matches the composition of many of the sediment samples from the Orca Basin brine pool and the surrounding inactive areas (Fig. 3). This match is consistent with the notion that biomass buried on the seafloor represents an isotopic archive of the nitrate that is dissolved in the overlying water column (Altabet and Francois, 1994; Tesdal et al., 2013). Nitrate is the major form of bioavailable nitrogen in the modern ocean, and nitrate-assimilating organisms adopt its isotopic composition, especially where nitrate is a limiting nutrient. In fact, this property has previously been exploited by Meckler et al. (2011), who investigated nitrogen isotopes in one core from Orca Basin with a depth range from 38-898 cm (*i.e.*, more extensive but at lower resolution than in this study) and used the data to draw inferences about the evolution of $\delta^{15}N$ in the marine nitrate pool over the past 25,000 years. Their results from the upper meter (< 3,000 years) are in good agreement with our data. The conclusion that these sediments archive the isotopic composition of marine nitrate in the form of nitrate-assimilating biomass is further supported by the strong correlation between TN and TOC with minimal TN intercept (grey and black data points in

Fig. 5), which indicates that most of the nitrogen in our sediment samples from the Orca Basin and surroundings is likely organic-bound or directly derived from biomass.

It has long been known that dissolved ammonium is highly enriched in the Orca Basin brine pool (Joye et al., 2005; Nigro et al., 2020; Van Cappellen et al., 1998; Wankel et al., 2010) compared to average seawater (< 0.1 µM, Cowen et al., 1998). Joye et al. (2005) attributed these high concentrations to three possible sources, including decomposition of sinking organic matter, desorption of ammonium from sinking inorganic particles, and desorption of ammonium from deeper sedimentary strata as the brine rises to the seafloor. Ammonium can adsorb to and become incorporated into clay minerals in substitution for potassium, as both ions have the same charge and similar radii (Abdulgawad et al., 2009; Yu et al., 2023). This substitution typically occurs during diagenesis, when ammonium is released from organic matter and appears in close contact with the sedimentary clay matrix (Müller, 1977; Schroeder and McLain, 1998). However, this process is salinity-dependent (Rysgaard et al., 1999; Yu et al., 2023), and therefore the high ionic strength of the brine that rises up through the sedimentary package may desorb ammonium that was previously stored in clay particles, possibly deeper down in the sediment column. Meckler et al. (2011) report bulk sedimentary $\delta^{15}N$ values up to 4 ‰ at 3 m depth, and so it is conceivable that the isotopic offset that we observed between the dissolved ammonium and the bulk sediments in our Orca Basin brine pool samples (core MUC_6, Fig. 6) represents upwards seepage of ammonium that was derived from sediments with a different isotopic composition. Alternatively, it is possible that the ammonium was derived from biomass or clays locally but with a small isotopic fractionation. For example, preferential degradation of isotopically enriched proteins relative to other biomolecules (Macko et al., 1987) may have generated an isotopically enriched ammonium pool in pore waters. Alternatively, the isotopic offset between dissolved ammonium and solid sediments may represent equilibrium fractionation between dissolved and adsorbed ammonium (Li et al., 2021).

Intriguingly, the ammonium $\delta^{15}N$ value of the top-most fluid sample from the Orca Basin brine core (MUC-6) is offset by 5.7 ‰ from its corresponding sediment sample (Fig. 6). Since we have only one data point, this observation is difficult to interpret. But if real, we speculate that it may represent a local biological effect, such as partial ammonium assimilation or nitrification/anammox. Ammonium assimilation imparts a fractionation of 14-27 ‰, rendering the residual ammonium isotopically heavy (Hoch et al., 1992; Waser et al.,

1998). Extremophiles residing in the brine pool may potentially perform this metabolism. While we did not find the corresponding isotopically light biomass of such ammonium-assimilating extremophiles in the Orca Basin sediments, it is possible that this component is swamped by the overwhelming influx of organic particles from above.

We note that core 4650-3 from the slope immediately surrounding the Orca Basin brine pool shows $\delta^{15}N$ values that are ca. 1-2 ‰ higher than the composition of marine nitrate, making this core distinct from all other cores from the Orca Basin. This core was taken above the halocline on the slope of the brine pool (Nigro et al., 2020) hence ammonium from the brine pool may have seeped into this sediment core. If so, then locally quantitative assimilation of isotopically enriched ammonium into biomass may explain the slightly elevated sedimentary $\delta^{15}N$ values. Interesting to note is that sponges, which occur at this site, are known to consume microbial biomass (Hanz et al., 2022), and hence N-fuelled microbial mats may drive sponge growth at this location.

In conclusion, the data from the Orca Basin brine pool and its surroundings support the notion that the isotopic composition of marine nitrate is well preserved in briny sedimentary organic matter. Furthermore, we find tentative evidence for biological utilization of the brine-sourced ammonium at the sediment-brine interface and in the surrounding slope setting that displays an unusually high activity of sponges.

5.2. Nitrogen redox cycling in active seeps near Dead Crab Lake

A striking feature of the active seep sediments near Dead Crab Lake compared to the sediments from within and around Orca Basin is the drop in $\delta^{15}N$ and C/N in the top few centimetres of all cores while both parameters are enriched at depth. The relatively elevated C/N ratios in the subsurface of these cores likely reflects leaching of ammonium by the saline fluids as they seep upwards. As noted above, ammonium is released from degrading biomass, and it tends to adsorb less strongly to clay minerals at high salinity. Previous studies have therefore speculated that seepage of saline fluids through the sediment package is an effective mechanism of exporting ammonium (Joye et al., 2005), and our data provide direct evidence for this process. The $\delta^{15}N$ enrichment in these subsurface sediments compared to background marine nitrate (Fig. 4) may thus represent a kinetic effect whereby isotopically light

ammonium is exported preferentially. (We note that this kinetic effect would counteract the equilibrium isotope effect discussed above in the context of core MUC-6 in the Orca brine pool).

The decrease in C/N in the core tops indicates enrichment in N compared to normal marine sediments, as represented by the sediment cores surrounding Orca Basin (Fig. 5). Previous studies identified microbial mats at the sampling site near Dead Crab Lake, including abundant sulfide oxidizers such as *Beggiatoa* that are known to actively accumulate nitrate in their cells (Salman-Carvalho et al., 2016; Stevens et al., 2015). It is likely that our sample preparation protocol washed out most nitrate from the samples; however, the N-enrichment may be a relic of biological nitrate uptake, if followed by conversion into organic-bound N.

The isotopic data provide additional insights into this process. In the core tops, $\delta^{15}N$ drops to values as low as -1.5 ‰ (Fig. 4). Such values fall within the range of biological N_2 fixation (Carpenter et al., 1997; Minagawa and Wada, 1986; Zerkle et al., 2008; Zhang et al., 2014). Usually, this metabolism occurs in settings characterized by N-limitation, but is has been described from benthic ammonium-rich environments where it is thought to serve as an electron sink (Knapp, 2012). Genomic evidence of the nitrogenase enzyme, which catalyzes N_2 fixation, has been described from an ammonium-rich brine seep in the Mediterranean where it may be involved in the production of osmo-protectants (Merlino et al., 2018; Pachiadaki et al., 2014). We cannot completely rule out this possibility as an explanation for the observed drop in $\delta^{15}N$ in our samples; however, it is not obvious why this process would be occurring preferentially at the sediment-water interface, which is also the interface between anoxic brine and oxic seawater (Teske and Joye, 2020), and not within Orca Basin or any of the slope sediments, which still contain dissolved ammonium above marine background.

Another possibility is partial ammonium assimilation by organisms that are feeding on the ammonium brought up by the brine seepage. This interpretation would be consistent with the drop in ammonium concentrations in the pore waters. As noted above, ammonium assimilation imparts a fractionation of 14-27 ‰ and may thus explain the production of isotopically light biomass (Hoch et al., 1992; Waser et al., 1998). However, this metabolism would generate isotopically enriched ammonium, while our measurements of $\delta^{15}N$ in pore waters show a decrease at the top, concurrent with the drop in sedimentary $\delta^{15}N$ (Fig. 5). Likewise, partial ammonium oxidation (aerobically or anaerobically) is expected to generate

isotopically heavy ammonium (Brunner et al., 2013; Casciotti et al., 2003), inconsistent with the fluid data.

Instead, the most parsimonious explanation for isotopically light ammonium is perhaps dissimilatory nitrate reduction to ammonium (DNRA). This metabolism imparts an isotopic fractionation of ca. 30 ‰, where the resulting ammonium is isotopically depleted (McCready et al., 1983). DNRA may be coupled to sulfide oxidation (Schutte et al., 2018), for which there is evidence in the Dead Crab Lake microbial mats (Stevens et al., 2015; Teske and Joye, 2020; Teske and Carvalho, 2020). The endmember brines are enriched in dissolved sulfide by a few mM (Salman-Carvalho et al., 2016). If nitrate-assimilating sulfide oxidizers reduce over 90% of their accumulated nitrate and store some of the resulting ammonium in their biomass, this could explain the observations (Fig. 7). If some of the resulting isotopically light ammonium is released and mixed with ambient ammonium from the brine, this process could explain our collective dataset, including the drop in sedimentary C/N and $\delta^{15}N$ as well as fluid $\delta^{15}N$. A smaller degree of nitrate reduction would also be possible if mixing between N-sources is taken into account. For example, 80% nitrate reduction by DNRA may generate biomass and ammonium with a composition around -10 ‰, which may be pushed up to the measured values if mixed with background biomass sinking down from the sea surface (2.5 ‰, see Orca Basin, Fig. 3) and with ammonium from the brine deeper in the same core (4.5 ‰, Fig. 6), respectively. In either case, the residual isotopically enriched nitrate (Fig. 7) would be small in abundance and become diluted by the larger marine nitrate reservoir.

One aspect that remains unexplained by this scenario is the drop in ammonium concentrations up-section in all cores, although DNRA generates additional ammonium. This drop may in part be explained by mixing between ammonium-rich brine and ammonium-poor seawater (Van Cappellen et al., 1998). However, the drop in ammonium in core 4652-5 is larger than the drop in electrical conductivity (factor of 3.3 versus 2.3), pointing towards an additional ammonium sink. We propose that this additional sink is (aerobic or anaerobic) ammonium oxidation above the sediment-water interface, given the strong redox gradient between the brine and the overlying water column (Teske and Joye, 2020). The isotopic effect of this process (1-25 ‰ for net oxidation of ammonium to nitrate, Casciotti, 2009), which should generate ammonium enriched in $\delta^{15}N$, is perhaps camouflaged by the isotopic signal of DNRA (30 ‰, McCready et al., 1983) that operates in the opposite direction. Genomic evidence of ammonium-oxidizing Archaea (AOA) has been retrieved from brine seeps in the

Red Sea and in the Mediterranean (Merlino et al., 2018), and ammonia-oxidizing archaea are abundantly associated with sulfur-oxidizing microbial mats and surficial sediments in Guaymas Basin (Engelen et al., 2021; Winkel et al., 2014). 16S rRNA gene sequences of ammonium-oxidizing Archaea have also been obtained from briny seep sediments in the Gulf of Mexico (Lloyd et al., 2006). Further evidence for oxidative processes at the sediment-water interface at our sampling site near Dead Crab Lake comes from the drop in $\delta^{13}C$, which may be indicative of methanotrophy (Grey, 2016).

In conclusion, our data suggest that in the active seep near Dead Crab Lake the influx of anoxic sulfide-rich brine stimulates DNRA at the brine-seawater interface, despite the presence of elevated ammonium concentrations in the brine fluid. However, we also see tentative evidence of ammonium consumption, possibly via aerobic or anaerobic oxidation. In any case, the concurrent drop in ammonium concentration and electrical conductivity shows that ammonium is mixed into the overlying water column. Here, it likely undergoes complete oxidation and mixing with the marine nitrate pool. The brine seeps near Dead Crab Lake thus constitute a source of recycled fixed nitrogen into marine environments.

5.3. Broader implications

Brine seeps enriched in base metals have been implicated in the formation of sediment-hosted ore deposits (Emsbo, 2009; Large et al., 1998; Sangster, 2018). In these settings, microbial activity at the brine-seawater interface may play a role in precipitating sulfide minerals of economic value (Lyons et al., 2006; Southam and Saunders, 2005). Similar to the brines in the Gulf of Mexico, ancient ore-forming fluids may have been enriched in ammonium that was leached from older sedimentary strata (Stüeken et al., 2021). The results from this study provide additional evidence of ammonium leaching by rising brine (Fig. 5), confirming previous hypotheses (Joye et al., 2005). In the context of ore-formation, where it is critical to maintain anoxic conditions via high microbial productivity, the provision of bioavailable ammonium by the metal-rich brines may be a key parameter. Previous work on a large economic SEDEX deposit in the McArthur Basin in Australia identified a 4‰ gradient in $\delta^{15}N$ with lower values (ca. 3.5 ‰) near the ore zone and higher values in more distal sediments (ca. 7.5 ‰) (Stüeken et al., 2021), which was at the time interpreted as hydrothermal nitrogen input with a light isotopic composition. The data from this work

indicate that such light values near the locality of brine injection may also result from secondary metabolisms, stimulated by brine-sourced metabolites.

The presence of brine seeps has further been invoked for the early Cambrian Burgess Shale environment that hosts some of the most famous animal fossils from the Cambrian explosion (Johnston et al., 2009; Powell et al., 2006). Dolomite and meter-scale chlinochlore laminates enriched in magnesium have been identified at several localities within the Burgess Shale Formation, which was deposited in a basinal environment. These enrichments are believed to represent anoxic Mg-rich brine pools that formed at the base of a carbonate platform escarpment. Although these brine pools have not been identified at every fossiliferous Burgess Shale outcrop locality, fossil distributions suggest that the pools concentrated megafauna around them as a result of increased microbial productivity (Johnston et al., 2009), possibly akin to the high activity of sponges seen in the slope setting in our study. We speculate that remobilized ammonium may have played a key role in driving this locally enhanced productivity. Burgess Shale Type preservation has been critical for our understanding of early Phanerozoic ecology (Gaines, 2014), preserving soft-bodied animals in exquisite detail (e.g., Parry and Caron, 2019), in addition to shelly fauna. The environmental factors that influence this type of preservation are key to recognising possible taphonomic biases in the rock record. The microbial and redox processes highlighted in this study provide an important reference point for interpreting taphonomic processes that may have operated around Cambrian brine seeps and influenced BST locally.

Lastly, our work highlights the difficulty of identifying DNRA in the sedimentary record. The isotopic trends at the brine-seawater interface at the active seep near Dead Crab Lake in the Gulf of Mexico can be linked to DNRA (Fig. 6), because we have the luxury of paired isotopic records of sedimentary biomass and dissolved ammonium, as well as support from previously published microbial observations and genomic data (Schutte et al., 2018; Stevens et al., 2015; Teske and Joye, 2020; Teske and Carvalho, 2020). In deep time, only the sedimentary record is available, and it would be difficult to reconstruct the presence of DNRA from this record alone, because the isotopic signature overlaps with that of other metabolisms. Our results therefore suggest that DNRA may be more prevalent at anoxic-oxic interfaces than previously thought. In fact, DNRA is a more efficient electron sink (eight electrons per nitrate molecule) compared to denitrification (five electrons per nitrate molecule), which may constitute an advantage when electron acceptors are limited (Teske,

2010). Tracking DNRA is further important, because unlike canonical denitrification or anammox, which both generate N_2 gas, DNRA retains bioavailable nitrogen in the system, making it advantageous for N-starved ecosystems. Widespread DNRA in the Precambrian ocean may thus help resolve a major nutrient limitation (Anbar and Knoll, 2002).

6. Conclusions

Modern brine seeps are important analogues for the formation of sedimentary exhalative ore deposits that host some of the major economic reserves of base metals (Large et al., 2005). They may also be important for understanding the distribution and preservation of animal fossils in the world-famous Burgess Shale (Gaines et al., 2012; Johnston et al., 2009). Both processes, *i.e.,* ore deposition and fossil preservation, are influenced by microbial activity and therefore require a thorough understanding of nutrient sources. Modern seep environments can thus serve as calibration points for nutrient fluxes and geochemical signatures that may be archived in the rock record.

Our data from the modern Gulf of Mexico, including the Orca Basin brine pool, its immediate surroundings, and an active seep are near Dead Crab Lake, support the notion that brine seeps carry with them bioavailable ammonium, mobilized from deeper sedimentary strata (Joye et al., 2005). While the modern ocean is relatively enriched in nitrate (ca. 30 μM, Gruber and Galloway, 2008), such a recycled ammonium flux from brine seeps may have constituted a major point source of a bio-essential nutrient in the Precambrian, when the ocean was likely N-depleted compared to today (Anbar and Knoll, 2002; Koehler et al., 2017; Stüeken et al., 2021), and it may have facilitated the preservation of animal fossils underneath microbial mats in the early Cambrian.

In this modern setting, where the brine-seawater interface is at the same time an interface between anoxic and oxic fluids (Teske and Joye, 2020), the brine seepage appears to stimulate dissimilatory nitrate reduction to ammonium (DNRA). We are able to infer this from paired sediment and fluid data and published genomic records; however, in the absence of the latter two datasets, which would typically be the case in studies of sedimentary rocks, it would be very difficult to prove the presence of this metabolism. DNRA may thus have been more common than previously thought along oxic-anoxic interfaces. Lastly, within the Orca Basin brine pool and its immediate surroundings, our isotopic data confirms that the composition of sinking biomass preserves the composition of seawater nitrate, as previously

proposed (Meckler et al., 2011). We also find tentative evidence of microbial ammonium recycling within the brine pool, but further analyses are required to confirm this proposition. In conclusion, our data add to growing evidence that brine seeps stimulate diverse microbial nitrogen metabolisms, which impact the sedimentary isotopic archive and may be preserved in ancient strata.

Acknowledgements

This work was financially supported by a NERC Frontiers grant (NE/V010824/1) and a Leverhulme Trust grant (RPG-2022-313) to EES. We thank Angus McLuskie for technical assistance. Sampling in the Gulf of Mexico was supported by NSF (Microbial Observatories 0801741). We thank the crew of RV *Atlantis* and HOV *Alvin* for expert performance during cruise AT18-02.

Open Research

All data generated in this project are presented in Tables 1-4 in the main text, and they are available from the National Geoscience Data Centre of the British Geological Survey under https://doi.org/10.5285/39988664-4361-4bee-a4ad-3f40931890c6.

Figures

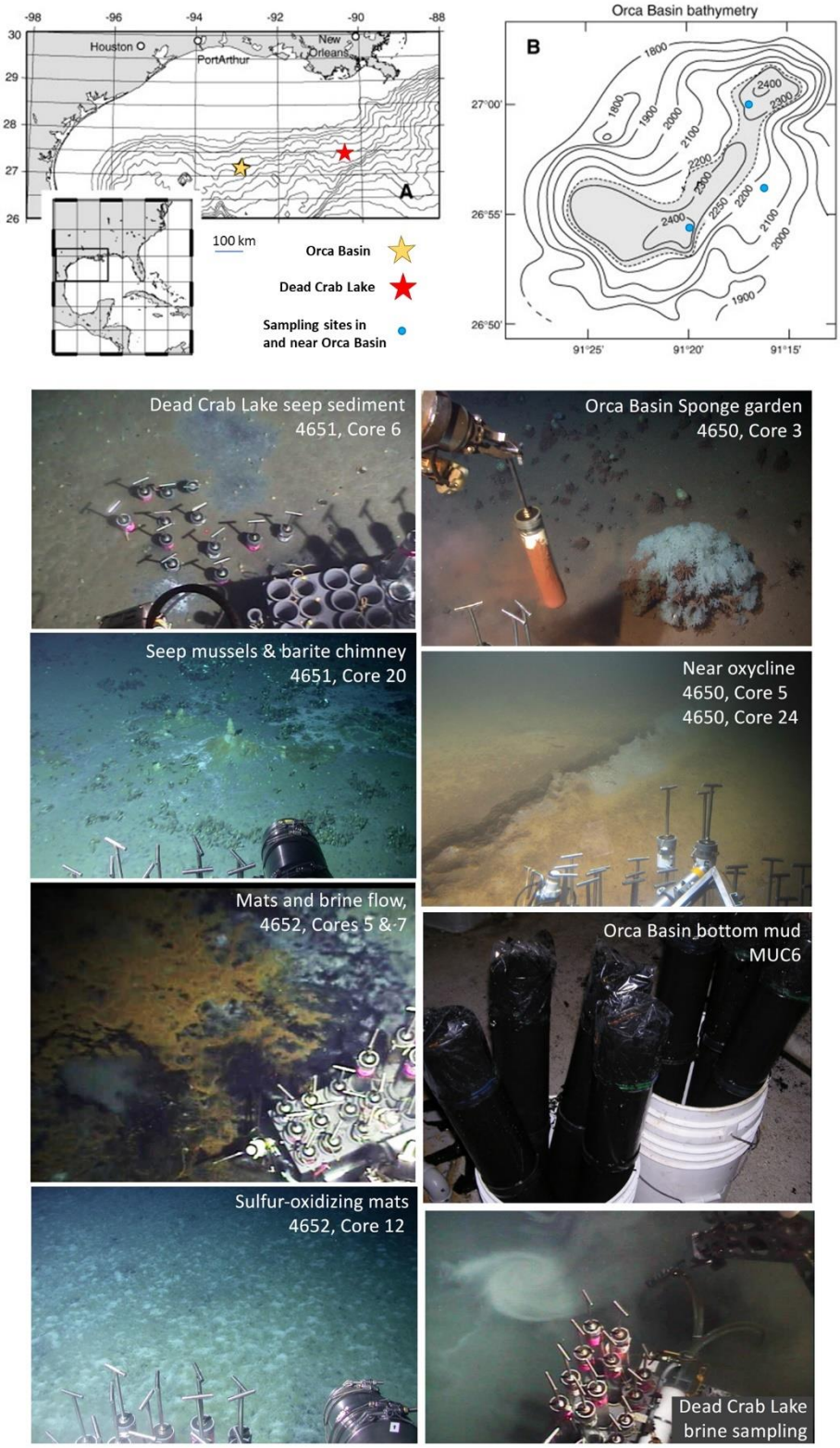

Figure 1: Map (top) and photos (bottom) showing sampling locations. *The map is modified from Tribovillard et al. (2008).*

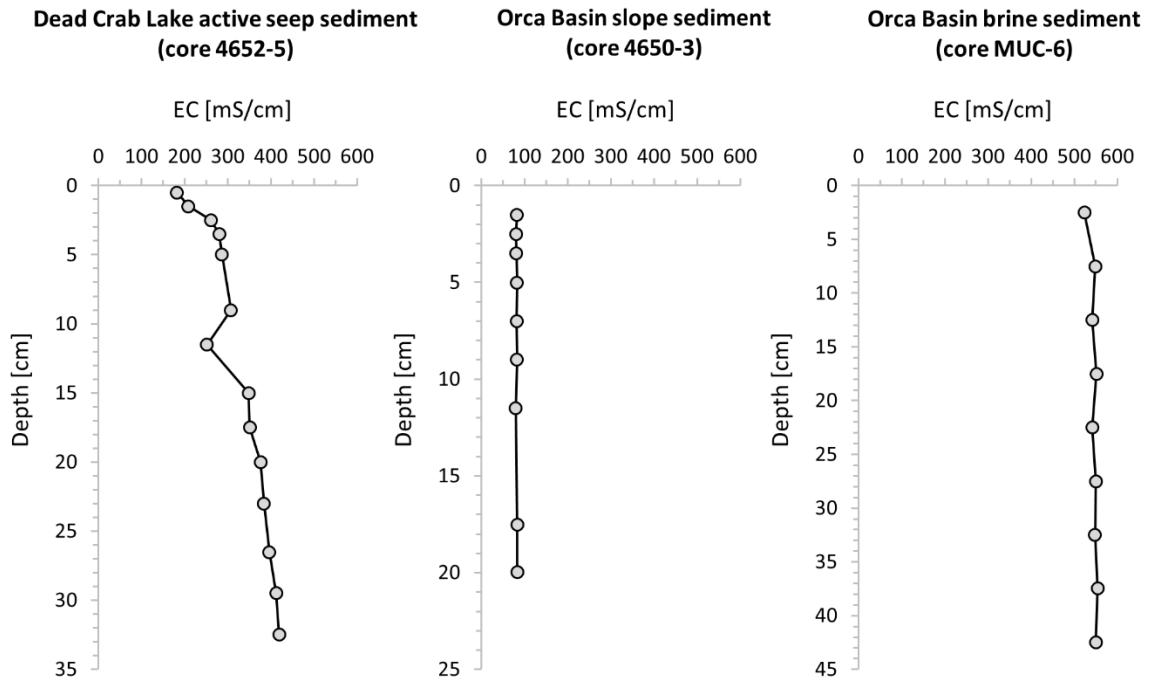

Figure 2: Electrical conductivity profiles. *Three representative cores from the three types of settings were chosen.*

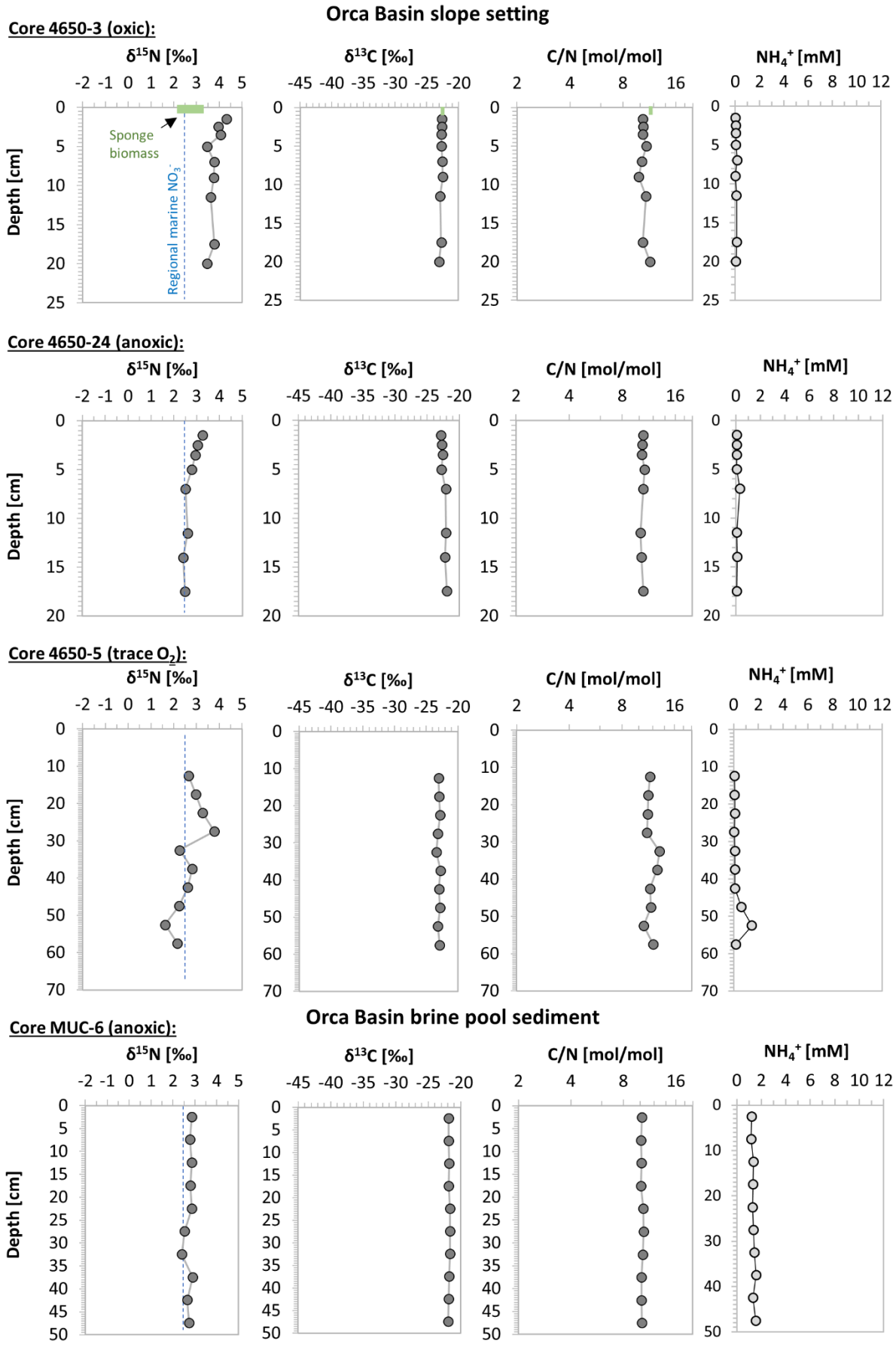
Orca Basin slope setting
Core 4650-3 (oxic):
Core 4650-24 (anoxic):
Core 4650-5 (trace O2):
Orca Basin brine pool sediment
Core MUC-6 (anoxic):
δ15N [‰]
δ13C [‰]
C/N [mol/mol]
NH4+ [mM]
Depth [cm]
Sponge biomass
Regional marine NO3-

618

Figure 3: Orca Basin sediments from the inactive pool surroundings and from the pool interior. *Sediment data were measured after removal of pore waters and after washing with HCl and DI-water. Vertical dashed blue line marks the composition of dissolved seawater nitrate in the Gulf of Mexico (Meckler et al., 2011). The sponge biomass shown for core 4650-3 represents material collected from the surface near the coring site. Dark grey = solid sedimentary material; light grey = pore fluids.*

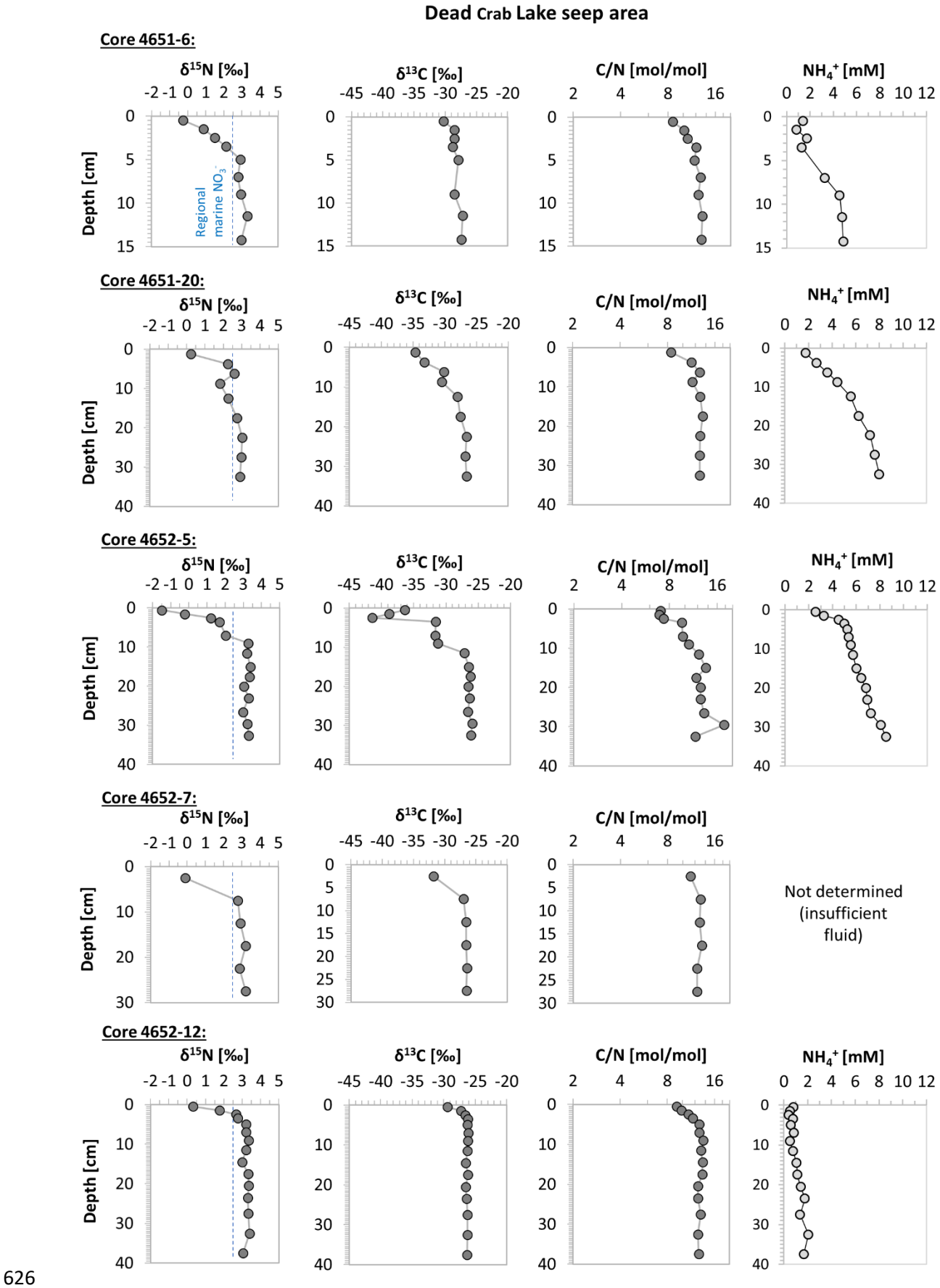
Dead Crab Lake seep area
Core 4651-6:
Core 4651-20:
Core 4652-5:
Core 4652-7:
Core 4652-12:
δ15N [‰]
δ13C [‰]
C/N [mol/mol]
NH4+ [mM]
Depth [cm]
Regional marine NO3-
Not determined (insufficient fluid)

626

Figure 4: Dead Crab Lake seeps, sediment profiles. *Vertical dashed blue line marks the composition of dissolved seawater nitrate in the Gulf of Mexico (Meckler et al., 2011). Symbol colours are as in Fig. 3.*

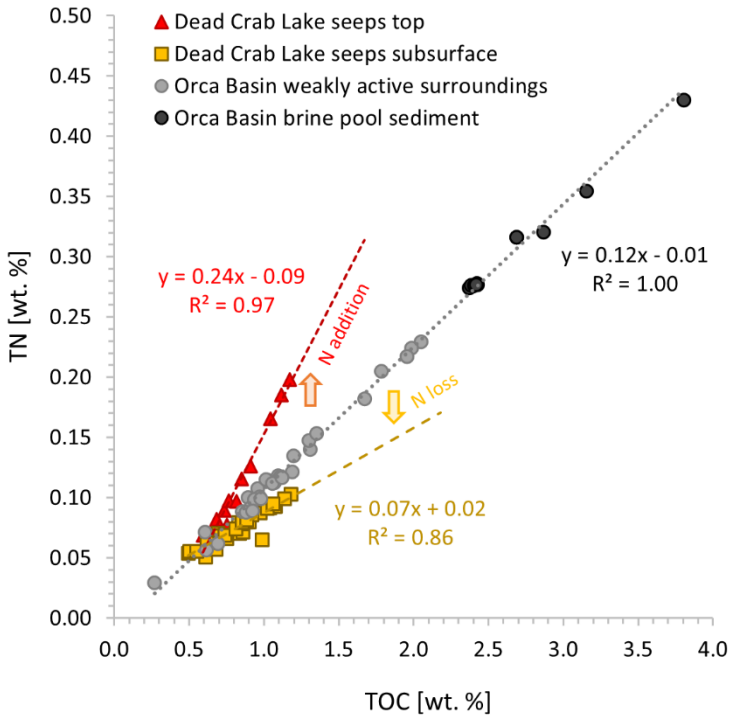

Figure 5: Total nitrogen versus total organic carbon in solids. *The shallow slope of the regression line through the subsurface samples from the seep near Dead Crab Lake (C/N > 10, yellow) suggests N loss relative to the core tops (C/N < 10, red). Dead Crab Lake core tops are enriched in N compared to the Orca Basin sediments.*

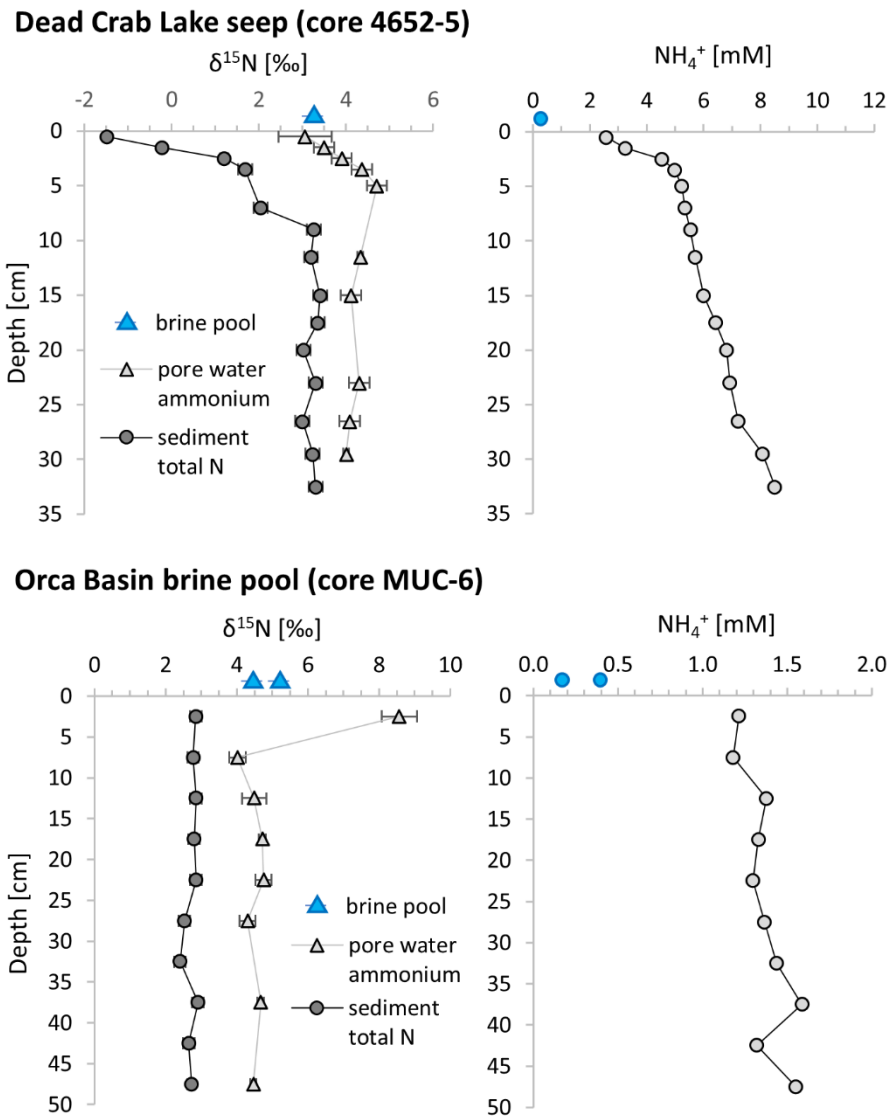

Figure 6: Isotopic comparison of dissolved ammonium and solid sedimentary nitrogen (left) along with dissolved ammonium concentrations (right) versus sediment depth*. The sedimentary nitrogen isotope data and the dissolved ammonium concentrations are replotted from Fig. 3 and 4. Error bars are ± 1 σ. Where replicates were not measured, the average standard deviation from all other samples is plotted. Blue data points show the compositions of the brine pool samples for comparison. The y-axis (sediment depth) does not apply to these samples. Note that the ammonium concentration of the brine pool like likely lower than that of the pore waters because the brine sample was taken from near the brine-seawater interface and is therefore more diluted by seawater.*

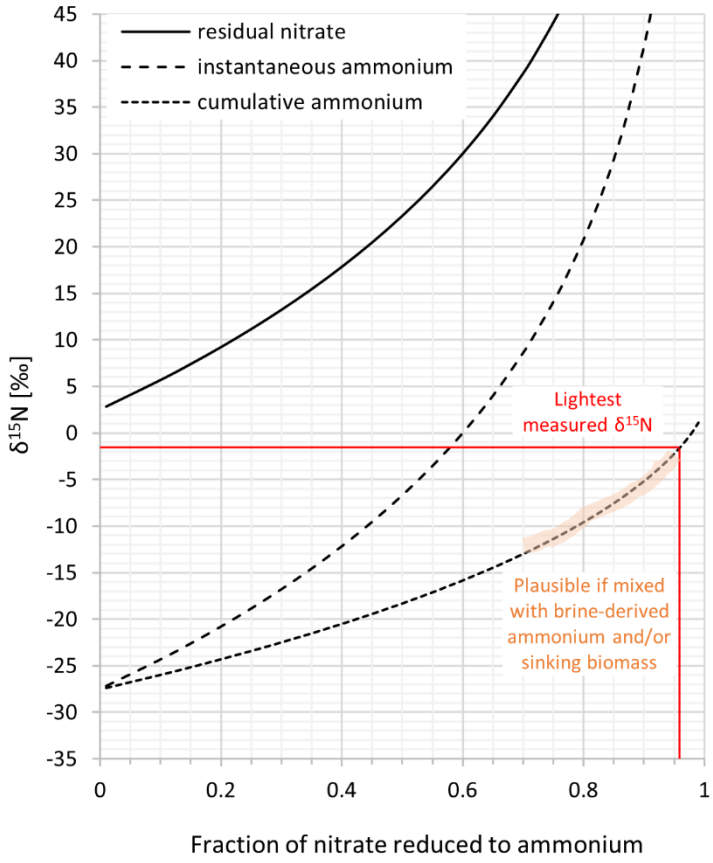

Figure 7: Rayleigh model of dissimilatory nitrate reduction to ammonium (DNRA). *The model is based on a fractionation of 30 ‰ and a starting composition of 2.5 ‰ for the initial nitrate (Meckler et al., 2011). With these parameters, over 90 % nitrate reduction are required to explain the light $\delta^{15}N$ value measured within biomass in the Dead Crab Lake seep sediments (Fig. 4). Lower degrees of reduction may be possible, if the resulting isotopically light ammonium is mixed with isotopically heavy ammonium coming up from the brine (Fig. 6) or, in the case of biomass, if it is mixed with sinking organic matter. Dissolved ammonium may further be pushed to heavier values by partial oxidation or assimilation (see text).*

666 ***Table 1: Electrical conductivity (EC) data from selected cores.***

Depth [cm]	EC [mS/cm]	Depth [cm]	EC [mS/cm]	Depth [cm]	EC [mS/cm]
Core 4652-5:		***Core 4650-3:***		***Core MUC-6:***	
0.5	182	1.5	82.4	2.5	524
1.5	208.3	2.5	80.4	7.5	549
2.5	260.9	3.5	80.8	12.5	542
3.5	280	5	82.4	17.5	552
5	286.7	7	81.5	22.5	542
9	307	9	82.2	27.5	550
11.5	251.8	11.5	79.3	32.5	548
15	348	17.5	82.9	37.5	554
17.5	351	20	82.8	42.5	550
20	376				
23	384				
26.5	396				
29.5	412				
32.5	419				

667

668 ***Table 2: Sediment data generated in this study.*** **These sample represent biomass collected from the sediment surface near the coring site.*
669 *Coordinates of sampling sites are provided as Latitude/Longitude.*

Sediment depth [cm]	$TOC_{sed.}$ [wt. %]	SD [wt. %]	$\delta^{13}C_{org}$ [‰]	SD [‰]	$TN_{sed.}$ [µg/g]	SD [µg/g]	$\delta^{15}N_{sed.}$ [‰]	SD [‰]	$C/N_{sed.}$ [mol/mol]	SD [mol/mol]	NH_4^+ [mM]	$\delta^{15}N_{NH4+}$ [‰]	SD [‰]
Active seep near Dead Crab Lake:													
Core 4651-6 (27N42.10/90W38.91, 834 m water depth):													
0.5	0.85	0.00	-30.28	0.12	1156	32	-0.27	0.15	8.57	0.24	1.406		
1.5	0.59		-28.51		685		0.86		10.11		0.842		
2.5	0.49		-28.50		540		1.51		10.67		1.740		
3.5	0.71		-28.81		683		2.13		12.12		1.300		
5.0	0.66		-27.90		655		2.92		11.81		n.d.		
7.0	0.88				799		2.79		12.86		3.272		
9.0	0.95		-28.54		886		2.94		12.46		4.547		
11.5	0.90		-27.19		796		3.30		13.21		4.759		
14.3	0.98		-27.40		873		2.97		13.06		4.860		
Core 4651-20 (27N42.10/90W38.91, 835 m water depth):													
1.25	0.91	0.17	-34.64	0.13	1261		0.24	0.01	8.43	0.06	1.745		
3.75	0.75	0.06	-33.23	0.39	773		2.25	0.16	11.34	0.17	2.662		
6.25	0.83		-30.09		791		2.61		12.79		3.596		
8.75	0.69		-30.49		704		1.82		11.50		4.446		
12.5	0.84		-27.99		703		2.28		12.90		5.576		
17.5	0.86		-27.51		712		2.73		13.36		6.252		
22.5	0.61		-26.53		503		3.04		12.89		7.217		
27.5	0.75		-26.74		663		2.99		12.81		7.607		
32.5	0.68		-26.57		571		2.91		12.81		7.982		
Core 4652-5 (27N42.10/90W38.91, 833 m water depth):													
0.5	1.12	0.03	-36.38	0.02	1850		-1.49	0.01	7.03	0.13	2.578	3.06	0.61
1.5	1.17	0.00	-38.78	0.02	1981		-0.23	0.01	6.89	0.04	3.246	3.49	
2.5	1.04	0.01	-41.41	0.32	1656		1.21	0.09	7.36	0.05	4.520	3.90	
3.5	0.73		-31.56		894		1.68		9.57		4.989	4.37	
5.0											5.228	4.70	

7.0	0.68		-31.65		821		2.04		9.69		5.341		
9.0	0.51		-31.27		556		3.26		10.60		5.538		
11.5	0.86		-27.11		820		3.20		12.28		5.712	4.33	0.07
15.0	1.08		-26.49		928		3.40		13.56		6.000	4.11	
17.5	0.69		-26.18		680		3.35		11.79		6.421		
20.0	0.74		-26.55		686		3.02		12.55		6.805		
23.0	0.87		-26.34		813		3.30		12.53		6.925	4.30	
26.5	1.04		-26.59		916		3.00		13.22		7.216	4.08	
29.5	0.99		-25.95		652		3.23		17.70		8.066	4.01	0.07
32.5	0.55		-26.14		553		3.30		11.66		8.498		
Core 4652-12 (27N42.09/90W38.87, 836 m water depth):													
0.5	0.76	0.00	-29.43	0.04	973	6	0.32	0.10	9.16	0.08	0.808		
1.5	0.82		-27.24		967		1.77		9.83		0.496		
2.5	0.63		-26.59		667		2.67		10.93		0.376		
3.5	0.62		-26.17		623		2.75		11.60		0.768		
5.0	0.86		-26.22		780		3.21		12.83		0.592		
7.0	0.81		-26.09		739		3.22		12.78		0.817		
9.0	1.07		-26.14		924		3.36		13.55		0.502		
11.5	1.02		-26.20		908		3.20		13.13		0.754		
14.5	1.18		-26.51		1025		3.01		13.43		1.063		
17.5	1.14		-26.18		991		3.32		13.38		1.122		
20.5	0.86		-26.49		801		3.36		12.53		1.418		
23.5	0.92		-26.34		854		3.30		12.53		1.759		
27.5	1.06		-26.21		949		3.33		13.02		1.362		
32.5	0.86		-26.24		794		3.39		12.57		2.051		
37.5	0.88	0.03	-26.32	0.03	813	17	3.04	0.01	12.68	0.18	1.675		
Core 4652-7 (27N42.10/90W38.91, 833 m water depth):													
2.5	0.80	0.01	-31.81	0.01	835	17	-0.11	0.23	11.21	0.07	n.d.		
7.5	0.85	0.01	-27.00	0.07	756	11	2.78	0.36	13.04	0.09	n.d.		
12.5	0.78		-26.54		707		2.93		12.86		n.d.		
17.5	0.91		-26.58		799		3.19		13.28		n.d.		

22.5	0.70		-26.46		656		2.88		12.37		n.d.
27.5	0.70		-26.53		660		3.21		12.36		n.d.
Slope site near Orca Basin:											
Core 4650-3 (sponges present, only oxic core from this site, 26N56.293/91W17.163, 2167 m water depth):											
1.5	1.20	0.02	-22.62	0.01	1348	1	4.32	0.18	10.35	0.16	0.010
2.5	1.03	0.03	-22.59	0.03	1145	18	3.95	0.05	10.47	0.11	0.049
3.5	0.96		-22.67		1076		4.07		10.37		0.063
5.0	1.31		-22.69		1401		3.47		10.91		0.075
7.0	1.01		-22.52		1152		3.78		10.25		0.156
9.0	0.60		-22.46		715		3.77		9.86		0.010
11.5	1.09		-22.90		1181		3.64		10.80		0.108
17.5	0.89		-22.72		1003		3.78		10.38		0.123
20.0	1.19		-23.01		1211		3.47		11.44		0.074
Core 4650-24 (no animals, anoxic, 26N56.29/91W17.16, 2198 m water depth):											
0*	1.11	0.01	-22.65	0.00	1171	16	3.37	0.13	11.04	0.08	0.062
0*	1.07		-22.47		1122		3.00		11.11		0.057
0*	1.06	0.14	-22.28	0.08	1120	150	2.37	0.01	11.01	0.02	0.058
0*	0.86	0.01	-22.42	0.03	885	14	2.03	0.59	11.28	0.01	0.063
1.5	1.96		-22.85		2173		3.25		10.50		0.075
2.5	2.05	0.04	-22.73	0.01	2295	64	3.05	0.35	10.41	0.08	0.081
3.5	1.98		-22.56		2240		2.95		10.33		0.084
5.0	1.67		-22.79		1823		2.78		10.71		0.076
7.0	1.96		-22.11		2171		2.51		10.51		0.338
11.5	1.78		-22.05		2046		2.62		10.17		0.085
14.0	1.30		-22.19		1475		2.41		10.30		0.086
17.5	1.35		-21.92		1532	34	2.49	0.26	10.50		0.120
Core 4650-5 (no animals, oxygen only in traces, 26N56.29/91W17.16, 2186 m water depth):											
12.5	0.91		-23.06		917		2.66		11.57		0.077
17.5	0.97	0.06	-22.93	0.29	1004	78	2.97	0.16	11.31	0.21	0.103
22.5	1.12	0.01	-22.84	0.10	1164	7	3.26	0.22	11.23	0.00	0.103
27.5	0.94	0.00	-23.19	0.14	982	0	3.79	0.28	11.11	0.04	0.062

32.5	0.69	0.05	-23.40	0.28	618	23	2.26	0.16	13.08	0.44	0.117		
37.5	0.62	0.03	-22.71	0.71	566	95	2.81	0.17	12.69	1.46	0.106		
42.5	0.98	0.01	-22.99	0.04	988	11	2.62	0.03	11.58	0.04	0.119		
47.5	0.88	0.04	-22.81	0.01	878	24	2.24	0.20	11.70	0.20	0.614		
52.5	0.27	0.09	-23.16	0.27	292	88	1.62	0.32	10.65	1.22	1.473		
57.5	0.92	0.04	-22.91	0.13	890	2	2.16	0.01	12.09	0.48	0.177		
Brine pool in Orca Basin:													
Core MUC-7 (27N00.00/91W16.99, 2350 m water depth):													
3	2.69		-21.79		3159		2.86		9.92		1.560		
Core MUC-6 (26N54.48/91W20.09, 2443 m water depth):													
2.5	2.43		-21.85		2769		2.85		10.22		1.213	8.57	0.49
7.5	2.37		-21.83		2739		2.77		10.10		1.180	4.02	
12.5	2.39		-21.82		2754		2.85		10.14		1.377	4.48	0.34
17.5	2.38		-21.85		2761		2.80		10.07		1.329	4.72	0.10
22.5	3.15		-21.65		3544		2.85		10.38		1.296	4.75	
27.5	2.87		-21.63		3201		2.53		10.45		1.366	4.30	
32.5	3.80		-21.64		4302		2.41		10.32		1.438		
37.5	2.42		-21.81		2775		2.91		10.18		1.586	4.67	0.09
42.5	2.41		-21.86		2761		2.65		10.16		1.320		
47.5	2.42	0.02	-21.91	0.03	2767	9	2.73	0.11	10.20	0.04	1.552	4.47	0.09

670

671 ***Table 3: Brine data from this study.*** *In the Orca Basin sites, the oxycline is at 2200 m water*
672 *depth. At the Dead Crab Lake site, the brine pool is shallow, so the sample was taken from*
673 *just below the brine pool surface.*

Water depth [m]	NH_4^+ [mM]	$\delta^{15}N_{NH4+}$ [‰]	SD [‰]
Orca Basin (Alvin dive 4647, 26N54.582/91W20.162)			
2235a	0.17	5.19	
2235b	0.18	5.13	0.18
Orca Basin (CTD cast 0502, 26N54.486/91W20.099)			
2240	0.36	4.24	0.15
2250	0.48	4.57	0.13
2300	0.49	4.70	0.60
Dead Crab L. (site 4651, 27N42.095/90W38.912)			
833	0.15	3.32	0.05

674
675

References

Abdulgawad F., Bockelmann E. B., Sapsford D., Williams K. P. and Falconer R. (2009) Ammonium ion adsorption on clays and sand under freshwater and seawater conditions. *Advances in Water Resources and Hydraulic Engineering*, 656-661.

Altabet M. A. and Francois R. (1994) Sedimentary nitrogen isotopic ratio as a recorder for surface ocean nitrate utilization. *Global Biogeochemical Cycles* **8**, 103-116.

Anbar A. D. and Knoll A. H. (2002) Proterozoic ocean chemistry and evolution: a bioinorganic bridge? *Science* **297**, 1137-1142.

Boetius A., Elvert M., Samarkin V. and Joye S. B. (2005) Molecular biogeochemistry of sulfate reduction, methanogenesis and the anaerobic oxidation of methane at Gulf of Mexico cold seeps. . *Geochimica et Cosmochimica Acta* **69**, 4267-4281.

Brandes J. A. and Devol A. H. (2002) A global marine-fixed nitrogen isotopic budget: Implications for Holocene nitrogen cycling. *Global Biogeochemical Cycles* **16**, doi: 10.1029/2001GB001856.

Brunner B., Contreras S., Lehmann M. F., Matantseva O., Rollog M., Kalvelage T., Klockgether G., Lavik G., Jetten M. S. M., Kartal B. and Kuypers M. M. (2013) Nitrogen isotope effects induced by anammox bacteria. *Proceedings of the National Academy of Sciences* **110**, 18994-18999.

Carpenter E. J., Harvey H. R., Fry B. and Capone D. G. (1997) Biogeochemical tracers of the marine cyanobacterium Trichodesmium. *Deep Sea Research Part I: Oceanographic Research Papers* **44**, 27-38.

Casciotti K. L. (2009) Inverse kinetic isotope fractionation during bacterial nitrite oxidation. *Geochimica et Cosmochimica Acta* **73**, 2061-2076.

Casciotti K. L., Sigman D. M. and Ward B. B. (2003) Linking diversity and stable isotope fractionation in ammonia-oxidizing bacteria. *Geomicrobiology Journal* **20**, 335-353.

Cleaves H. J., Chalmers J. H., Lazcano A., Miller S. L. and Bada J. L. (2008) A reassessment of prebiotic organic synthesis in neutral planetry atmospheres. *Origins of Life and Evolution of Biospheres* **38**, 105-115.

Cowen J. P., Wen X., Jones R. D. and Thomson R. E. (1998) Elevated NH_4^+ in a neutrally buoyant hydrothermal plume. *Deep Sea Research Part I: Oceanographic Research Papers* **45**, 1891-1902.

Dennen K. O., Johnson C. A., Otter M. L., Silva S. R. and Wandless G. A. (2006) $\delta^{15}N$ and non-carbonate $\delta^{13}C$ values for two petroleum source rock reference materials and a marine sediment reference material. *U.S. Geological Survey Open-File Report 2006-1071*.

Emsbo P. (2009) Geologic criteria for the assessment of sedimentary exhalative (sedex) Zn-Pb-Ag deposits. *US Geological Survey open-file report* **1209**, 1-21.

Engelen B., Nguyen T., Heyerhoff B., Kalenborn S., Sydow K., Tabai H., Peterson R. N., Wegener G. and Teske A. (2021) Microbial Communities of Hydrothermal Guaymas Basin Surficial Sediment Profiled at 2 Millimeter-Scale Resolution. *Frontiers in Microbiology* **12**, doi: 10.3389/fmicb.2021.710881

Gaines R. R. (2014) Burgess Shale-type preservation and its distribution in space and time. *The Paleontological Society Papers* **20**, 123-146.

Gaines R. R., Hammarlund E. U., Hou X., Qi C., Gabbott S. E., Zhao Y., Peng J. and Canfield D. E. (2012) Mechanism for Burgess Shale-type preservation. *Proceedings of the National Academy of Sciences* **109**, 5180-5184.

Gonzalez C. A. and Choquette S. J. (2023) Reference Material 8547, IAEA-N-1 (Nitrogen Isotopes in Ammonium Sulfate), Reference Material Information Sheet. National Institute of Standards and Technology (NIST), US Department of Commerce, pp. 1-5.

Grey J. (2016) The incredible lightness of being methane-fuelled: stable isotopes reveal alternative energy pathways in aquatic ecosystems and beyond. *Frontiers in Ecology and Evolution* **4**, doi: 10.3389/fevo.2016.00008.

Gruber N. and Sarmiento J. L. (1997) Global patterns of marine nitrogen fixation and denitrification. *Global Biogeochemical Cycles* **11**, 235-266.

Gruber N. and Galloway J. N. (2008) An Earth-system perspective of the global nitrogen cycle. *Nature* **451**, 293-296.

Hanz U., Riekenberg P., de Kluijver A., van der Meer M., Middelburg J. J., de Goeij J. M., Bart M. C., Wurz E., Colaço A., Duineveld G. C. and Reichart G. J. (2022) The important role of sponges in carbon and nitrogen cycling in a deep-sea biological hotspot. *Functional Ecology* **36**, 2188-2199.

Hoch M. P., Fogel M. L. and Kirchman D. L. (1992) Isotope fractionation associated with ammonium uptake by a marine bacterium. *Limnology and Oceanography* **37**, 1447-1459.

Ireland T., Large R. R., McGoldrick P. and Blake M. (2004) Spatial distribution patterns of sulfur isotopes, nodular carbonate, and ore textures in the McArthur River (HYC) Zn-Pb-Ag deposit, Northern Territory, Australia. *Economic Geology* **99**, 1687-1709.

Johnston P. A., Johnston K. J., Collom C. J., Powell W. G. and Pollock R. J. (2009) Palaeontology and depositional environments of ancient brine seeps in the Middle Cambrian Burgess Shale at The Monarch, British Columbia, Canada. *Palaeogeography, Palaeoclimatology, Palaeoecology* **277**, 86-105.

Joye S. B., MacDonald I. R., Montoya J. P. and Peccini M. (2005) Geophysical and geochemical signatures of Gulf of Mexico seafloor brines. *Biogeosciences* **2**, 295-309.

Joye S. B., Bowles M. W., Samarkin V. A., Hunter K. S. and Niemann H. (2010) Biogeochemical signatures and microbial activity of different cold-seep habitats along the Gulf of Mexico deep slope. *Deep Sea Research Part II: Topical Studies in Oceanography* **57**, 1990-2001.

Knapp A. N. (2012) The sensitivity of marine N2 fixation to dissolved inorganic nitrogen. *Frontiers in Microbiology* **3**, doi: 10.3389/fmicb.2012.00374.

Knapp A. N., Sigman D. M. and Lipschultz F. (2005) N isotopic composition of dissolved organic nitrogen and nitrate at the Bermuda Atlantic Time-series Study site. *Global Biogeochemical Cycles* **19**, doi: 10.1029/2004GB002320.

Koehler M. C., Stüeken E. E., Kipp M. A., Buick R. and Knoll A. H. (2017) Spatial and temporal trends in Precambrian nitrogen cycling: a Mesoproterozoic offshore nitrate minimum. *Geochimica et Cosmochimica Acta* **198**, 315-337.

Large R. R., Bull S. W., Cooke D. R. and McGoldrick P. J. (1998) A genetic model for the HYC Deposit, Australia; based on regional sedimentology, geochemistry, and sulfide-sediment relationships. *Economic Geology* **93**, 1345-1368.

Large R. R., Bull S. W., McGoldrick P. J. and Walters S. G. (2005) Stratiform and strata-bound Zn-Pb-Ag deposits in Proterozoic sedimentary basins, northern Australia. *Economic Geology* **100**, 931-963.

Li Y., Li L. and Wu Z. (2021) First-principles calculations of equilibrium nitrogen isotope fractionations among aqueous ammonium, silicate minerals and salts. *Geochimica et Cosmochimica Acta* **297**, 220-232.

Lloyd K. G., Lapham L. and Teske A. (2006) An anaerobic methane-oxidizing community of ANME-1 archaea in hypersaline Gulf of Mexico sediments. *Applied and Environmental Microbiology* **72**, 7218-7230.

774 Lloyd K. G., Albert D. B., Biddle J. F., Chanton J. P., Pizarro O. and Teske A. (2010) Spatial
775 structure and activity of sedimentary microbial communities underlying a Beggiatoa
776 spp. mat in a Gulf of Mexico hydrocarbon seep. *PLoS ONE* **5**, e8738.
777 Lyons T. W., Gellatly A. M., McGoldrick P. J. and Kah L. C. (2006) Proterozoic sedimentary
778 exhalative (SEDEX) deposits and links to evolving global ocean chemistry. In
779 *Evolution of early Earth's atmosphere, hydrosphere, and biosphere - constraints from*
780 *ore deposits* (eds. S. E. Kesler and H. Ohmoto). Geological Society of America
781 Memoir.
782 Macko S. A., Fogel M. L., Hare P. E. and Hoering T. C. (1987) Isotopic fractionation of
783 nitrogen and carbon in the synthesis of amino acids by microorganisms. *Chemical*
784 *Geology* **65**, 79-92.
785 Mapelli F., Barozzi A., Michoud G., Merlino G., Crotti E., Borin S. and Daffonchio D. (2017)
786 An updated view of the microbial diversity in deep hypersaline anoxic basins. In
787 *Adaption of microbial life to environmental extremes: Novel research results and*
788 *application* (eds. H. Stan-Lotter and S. Fendrihan). Springer Link. pp. 23-40.
789 Marconi D., Weigand M. A. and Sigman D. M. (2019) Nitrate isotopic gradients in the North
790 Atlantic Ocean and the nitrogen isotopic composition of sinking organic matter. *Deep*
791 *Sea Research Part I: Oceanographic Research Papers* **145**, 109-124.
792 McCready R. G. L., Gould W. D. and Barendregt R. W. (1983) Nitrogen isotope fractionation
793 during the reduction of NO3-to NH4+ by Desulfovibrio sp. *Canadian Journal of*
794 *Microbiology* **29**, 231-234.
795 Meckler A. N., Ren H., Sigman D. M., Gruber N., Plessen B., Schubert C. J. and Haug G. H.
796 (2011) Deglacial nitrogen isotope changes in the Gulf of Mexico: Evidence from bulk
797 sedimentary and foraminifera-bound nitrogen in Orca Basin sediments.
798 *Paleoceanography* **26**, doi: 10.1029/2011PA002156.
799 Merlino G., Barozzi A., Michoud G., Ngugi D. K. and Daffonchio D. (2018) Microbial
800 ecology of deep-sea hypersaline anoxic basins. *FEMS Microbiology Ecology* **94**, doi:
801 10.1093/femsec/fiy1085.
802 Minagawa M. and Wada E. (1986) Nitrogen isotope ratios of red tide organisms in the East
803 China Sea: a characterization of biological nitrogen fixation. *Marine Chemistry* **19**,
804 245-259.
805 Müller P. J. (1977) CN ratios in Pacific deep-sea sediments: Effect of inorganic ammonium
806 and organic nitrogen compounds sorbed by clays. *Geochimica et Cosmochimica Acta*
807 **41**, 765-776.
808 Nigro L. M., Elling F. J., Hinrichs K. U., Joye S. B. and Teske A. (2020) Microbial ecology
809 and biogeochemistry of hypersaline sediments in Orca Basin. *PLoS One* **15**, doi:
810 10.1371/journal.pone.0231676.
811 Pachiadaki M. G., Yakimov M. M., LaCono V., Leadbetter E. and Edgcomb V. (2014)
812 Unveiling microbial activities along the halocline of Thetis, a deep-sea hypersaline
813 anoxic basin. *The ISME Journal* **8**, 2478-2489.
814 Parry L. and Caron J. B. (2019) Canadia spinosa and the early evolution of the annelid
815 nervous system. *Science Advances* **5**, eaax5858.
816 Peel F. J., Travis C. J. and Hossack J. R. (1995) Genetic structural provinces and salt
817 tectonics of the Cenozoic offshore U.S. Gulf of Mexico: a preliminary analysis. In
818 *Salt Tectonics: a Global Perspective* (eds. J. M.P.A., R. D.G. and S. S.). AAPG. pp.
819 153-175.
820 Pilcher R. S. and Blumstein R. D. (2007) Brine volume and salt dissolution rates in Orca
821 Basin, northeast Gulf of Mexico. *AAPG Bulletin* **91**, 823-833.

Pindell J. L. and Kennan L. (2009) Tectonic evolution of the Gulf of Mexico, Caribbean and northern South America in the mantle reference frame: an update. *Geological Society, London, Special Publications* **328**, 1-55.

Powell W. G., Johnston P. A., Collom C. J. and Johnston K. J. (2006) Middle Cambrian brine seeps on the Kicking Horse Rim and their relationship to talc and magnesite mineralization and associated dolomitization, British Columbia, Canada. *Economic Geology* **101**, 431-451.

Roberts H. H. and Carney R. S. (1997) Evidence of episodic fluid, gas, and sediment venting on the northern Gulf of Mexico continental slope. *Economic Geology* **92**, 863-879.

Rysgaard S., Thastum P., Dalsgaard T., Christensen P. B. and Sloth N. P. (1999) Effects of salinity on NH 4+ adsorption capacity, nitrification, and denitrification in Danish estuarine sediments. *Estuaries* **22**, 21-30.

Salman-Carvalho V., Fadeev E., Joye S. B. and Teske A. (2016) How clonal is clonal? Genome plasticity across multicellular segments of a "Candidatus Marithrix sp." filament from sulfidic, briny seafloor sediments in the Gulf of Mexico. *Frontiers in Microbiology* **7**, doi: 10.3389/fmicb.2016.01173.

Sangster D. F. (2018) Toward an integrated genetic model for vent-distal SEDEX deposits. *Mineralium Deposita* **53**, 509-527.

Sassen R., Roberts H., Aharon R., Larkin J., Chinn E. and Carney R. (1993) Chemosynthetic bacterial mats at cold hydrocarbon seeps Gulf of Mexico continental slope. *Organic Geochemistry* **20**, 77-89.

Schimmelmann A., Qi H., Coplen T. B., Brand W. A., Fong J., Meier-Augenstein W., Kemp H. F., Toman B., Ackermann A., Assonov S. and Aerts-Bijma A. T. (2016) Organic reference materials for hydrogen, carbon, and nitrogen stable isotope-ratio measurements: caffeines, n-alkanes, fatty acid methyl esters, glycines, L-valines, polyethylenes, and oils. *Analytical Chemistry* **88**, 4294-4302.

Schroeder P. A. and McLain A. A. (1998) Illite-smectites and the influence of burial diagenesis on the geochemical cycling of nitrogen. *Clay Minerals* **33**, 539-546.

Schutte C. A., Teske A., MacGregor B. J., Salman-Carvalho V., Lavik G., Hach P. and de Beer D. (2018) Filamentous Giant Beggiatoaceae from the Guaymas Basin Are Capable of both Denitrification and Dissimilatory Nitrate Reduction to Ammonium. *Applied Environmental Microbiology* **84**, doi: 10.1128/AEM.02860-02817.

Shokes R. F., Trabant P. K., Presley B. J. and Reid D. F. (1977) Anoxic, Hypersaline Basin in the Northern Gulf of Mexico. *Science* **196**, 1443-1446.

Sigman D. M., Altabet M. A., McCorkle D. C., Francois R. and Fischer G. (2000) The d15N of nitrate in the southern ocean: nitrogen cycling and circulation in the ocean interior. *Journal of Geophysical Research* **105**, doi: 10.1029/2000JC000265.

Southam G. and Saunders J. A. (2005) The geomicrobiology of ore deposits. *Economic Geology* **100**, 1067-1084.

Stevens E. N., Bailey J. V., Flood B. E., Jones D. W., Gilhooly III W. P., Joye S. B., Teske A. and Mason O. U. (2015) Barite encrustation of benthic sulfide-oxidizing bacteria at a marine cold seep. *Geobiology* **13**, 588-603.

Stüeken E. E., Gregory D. D., Mukherjee I. and McGoldrick P. (2021) Sedimentary exhalative venting of bioavailable nitrogen into the early ocean. *Earth and Planetary Science Letters* **565**, doi: 10.1016/j.epsl.2021.116963.

Tesdal J. E., Galbraith E. D. and Kienast M. (2013) Nitrogen isotopes in bulk marine sediment: linking seafloor observations with subseafloor records. *Biogeosciences* **10**, 101-118.

Teske A. (2010) Cryptic links in the ocean. *Science* **330**, 1326-1327.

Teske A. and Joye S. B. (2020) The Gulf of Mexico: An introductory survey of a seep-dominated seafloor landscape. In *Marine Hydrocarbon Seeps: Microbiology and Biogeochemistry of a Global Marine Habitat* (eds. A. Teske and V. Carvalho). Springer Link. pp. 69-100.

Teske A. and Carvalho V. (2020) Large sulfur-oxidizing bacteria at Gulf of Mexico hydrocarbon seeps. In *Marine Hydrocarbon Seeps: Microbiology and Biogeochemistry of a Global Marine Habitat* (eds. A. Teske and V. Carvalho). Springer Link. pp. 149-171.

Tribovillard N., Bout-Roumazeilles V., Algeo T., Lyons T. W., Sionneau T., Montero-Serrano J. C., Riboulleau A. and Baudin F. (2008) Paleodepositional conditions in the Orca Basin as inferred from organic matter and trace metal contents. *Marine Geology* **254**, 62-72.

Van Cappellen P., Viollier E., Roychoudhury A., Clark L., Ingall E., Lowe K. and Dichristina T. (1998) Biogeochemical cycles of manganese and iron at the oxic− anoxic transition of a stratified marine basin (Orca Basin, Gulf of Mexico). *Environmental Science and Technology* **32**, 2931-2939.

Wankel S. D., Joye S. B., Samarkin V. A., Shah S. R., Friederich G., Melas-Kyriazi J. and Girguis P. R. (2010) New constraints on methane fluxes and rates of anaerobic methane oxidation in a Gulf of Mexico brine pool via in situ mass spectrometry. *Deep Sea Research Part II: Topical Studies in Oceanography* **57**, 2022-2020.

Waser N. A. D., Harrison P. J., Nielsen B., Calvert S. E. and Turpin D. H. (1998) Nitrogen isotope fractionation during the uptake and assimilation of nitrate, nitrite, ammonium, and urea by a marine diatom. *Limnology and Oceanography* **43**, 215-224.

Williams N. (1978) Studies of the base metal sulfide deposits at McArthur River, Northern Territory, Australia; II, The sulfide-S and organic-C relationships of the concordant deposits and their significance. *Economic Geology* **73**, 1036-1056.

Williford K. H., Grice K., Logan G. A., Chen J. and Huston D. (2011) The molecular and isotopic effects of hydrothermal alteration of organic matter in the Paleoproterozoic McArthur River Pb/Zn/Ag ore deposit. *Earth and Planetary Science Letters* **301**, 382-392.

Winkel M., De Beer D., Lavik G., Peplies J. and Mussmann M. (2014) Close association of active nitrifyers with Beggiatoa mats covering deep-sea hydrothermal sediments. *Environmental Microbiology* **16**, 1612-1626.

Yu A. J., Lin X., Zhu J., He H. and Li L. (2023) Environmental effects on ammonium adsorption onto clay minerals: Experimental constraints and applications. *Applied Clay Science* **246**, doi: 10.1016/j.clay.2023.107165.

Zerkle A., Junium C. K., Canfield D. E. and House C. H. (2008) Production of ^{15}N-depleted biomass during cyanobacterial N_2-fixation at high Fe concentrations. *Journal of Geophysical Research* **113**, doi: 10.1029/2007JG000651.

Zhang S., Fang Y. and Xi D. (2016) Adaptation of micro-diffusion method for the analysis of 15N natural abundance of ammonium in samples with small volume. *Rapid Communications in Mass Spectrometry* **29**, 1297-1306.

Zhang X., Sigman D. M., Morel F. M. and Kraepiel A. M. (2014) Nitrogen isotope fractionation by alternative nitrogenases and past ocean anoxia. *Proceedings of the National Academy of Sciences* **111**, 4782-4787.